ACS EARTH AND SPACE CHEMISTRY

http://pubs.acs.org/journal/aesccq

Letter

Conformer Distributions of *n*-Propyl Cyanide in the Gas Phase and Following Ice Sublimation Measured by Broadband Rotational Spectroscopy

Anudha Kanaherarachchi, Travis Hager, Quentin Borengasser, and Bernadette M. Broderick*

Cite This: *ACS Earth Space Chem.* 2024, 8, 14–20

Read Online

ACCESS | Metrics & More | Article Recommendations | Supporting Information

ABSTRACT: The conformer distribution of *normal*-propyl cyanide is investigated using broadband chirped pulse rotational spectroscopy in the millimeter-wave regime coupled with buffer gas cooling. Here we explore the relative abundances of the *anti* and *gauche* conformers following room-temperature gas-phase injection into a 25 K buffer gas cell and compare to that which is observed following temperature-programmed desorption from an ice surface, similar to the slow warm-up experienced by ice grains as they approach warmer regions within the interstellar medium. The conformer distributions observed in the gas phase from room-temperature injection are then used to determine their relative energies, an important parameter needed to interpret the isomer and conformer abundances derived from astronomical observations. We find the *gauche* conformer to be the most stable species by ∼97 ± 21 cm^{-1}. We further examine the relative conformer abundances following ice desorption, which are distinct from those following the gas-phase introduction. The ratios measured off the ice correspond to a conformer temperature of ∼56 K, which is much lower than their sublimation temperature of 170 K.

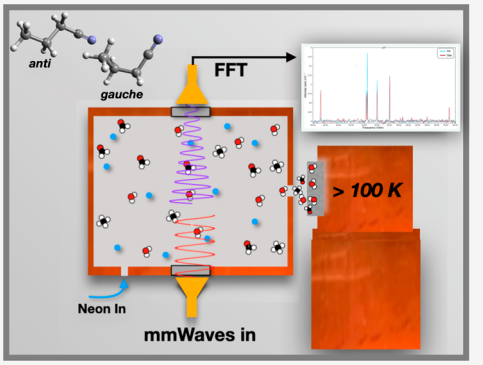

KEYWORDS: *conformers, chirped-pulse mm-wave spectroscopy, interstellar ice grains, temperature-programmed desorption, sublimation*

INTRODUCTION

As of June 2023, ∼300 molecules of rich chemical diversity have been detected in the interstellar medium (ISM) or circumstellar shells.[1,2] Furthermore, more than 80 different amino acids have been discovered in meteorites found on Earth.[3−6] The suspicion that the latter molecules or their precursors were formed in the ISM has brought about an era of exploration and an investigation for the molecular candidates and formation pathways that could explain these findings. In the search for precursors to amino acids, emphasis is given to molecules containing nitrogen, often as −CN groups. By now, more than 30 different molecules containing −CN groups have been discovered in the ISM.[1,2]

Propyl cyanide (hereafter referred to as PrCN) exists in two structural isomers: *normal*-propyl cyanide (*n*-PrCN) and *iso*-propyl cyanide (*i*-PrCN). There are two conformers of the *n*-PrCN species: the *anti* form (−CN group attached to the CCC plane at the terminal carbon, trans to the CCC chain) and the *gauche* form (CN group attached to the CCC plane at the terminal carbon, rotated by ±120° to the CCC plane), both of which have been observed in the ISM. The *anti* species was the first of the *n*-PrCN conformers to be detected in 2009 with IRAM[7] near the main hot core of SgrB2(N). Subsequently, both conformers were detected during the EMOCA survey with the Atacama Large Millimeter/Submillimeter Array (ALMA) around SgrB2(N2), in the more northerly hot core of the two in SgrB2(N) identified at the time.[8] The first detection of *i*-PrCN also occurred during this survey around SgrB2(N2). The *iso*/*n* ratio within this region was determined to be 0.4 (±0.06). Shortly after, both species were detected within Orion KL by Pagani and co-workers with varying *iso*/*n* ratios across several emission peaks.[9] They reported an *iso*/*n* ratio of 0.5 in IRc21, 0.33 in MF10, and 0.16 in MF2.

The full mechanistic picture by which these molecules are produced in star-forming regions has not yet emerged, although it is widely accepted that chemistry on icy grain mantles is key. Investigations via chemical models and ever improving reaction networks have yielded results which appear to converge on several aspects of the formation of *n*-PrCN and *i*-PrCN. Based on previous work by himself and others,[10−13] Garrod introduced the chemical kinetic model (MAGICKAL) designed to simulate physical and chemical conditions of hot cores,[14] which was later used to investigate the formation of PrCN in Sgr(B2), obtaining varying *iso*/*normal* ratios for the

Received: November 17, 2023
Revised: December 18, 2023
Accepted: December 28, 2023
Published: January 2, 2024

different isomer species. At first the ratio was determined to be 2.2,[8] which at the time was quite different from the observed value of 0.4. Upon improving the chemical network years later, they were able to produce *iso*/*normal* values ranging from 0.17 to 3.0 based on different conditions applied.[15] In both cases, the addition of a CH_3 radical to an unsaturated alkyl cyanide and the addition of a CN radical to an unsaturated hydrocarbon were found to be major contributors to the formation of the two PrCN isomers. More recently, they made further changes to the chemical model and examined the formation of PrCN and propanol (PrOH).[16] In that work, they removed the feature of bulk diffusion of heavy species (all species other than H and H_2). This change affected the reaction pathways which included CN radicals, and as a result, in contrast to the findings from 2017, they found that the reaction between the CN radical and propene is in fact not an important mechanism for PrCN formation. However, the insertion of CH_2 into ethyl cyanide (EtCN) was again found to be a major contributor to the *n*- and *iso*-PrCN formation on ice surfaces. During these reactions on surfaces, *i*-PrCN is slower to form than *n*-PrCN because CH_3 insertion to EtCN (initiated by H abstraction) favors the formation of *n*-PrCN. However, as the reaction progresses, the addition of a CH_3 group to H-abstracted C_2H_5CN becomes the more favored reaction for PrCN formation. This causes the production of *i*-PrCN to become dominant. Recent work on the formation of PrCN isomers with DFT methods using M062X and ωB97XD functionals with the 6-311 ++ G(d,p) basis set by Kerkeni and co-workers reports agreement with the formation pathways with cyanide addition and alkyl addition to alkyl cyanides on ice surfaces.[17] However, given the range of assumptions made and outcomes found, it is clear that the models can benefit from additional detailed experimental guidance.

In addition to the wide range of studies focused on the formation pathways of PrCN, determination of the relative energies of the *anti* and *gauche* conformers of the *n*-PrCN species has also been the subject of both computational and experimental investigations. MW/mm-wave studies of vibrational ground state PrCN from Hirota suggested that the *anti* species is the lower energy conformer based on the intensity of the *anti* and *gauche* spectra and inferred that the energy difference is likely less than 350 cm^{-1}.[18] Subsequent gas-phase mm-wave studies of *n*-PrCN by Wlodarczak and co-workers reported an energy difference of 91 ± 25.1 cm^{-1} with the *anti* species again being the more stable conformer.[19] This energy difference was calculated using peak absorption coefficients for asymmetric tops and the line width at half intensity as it was shown for 2-amino-1-propanol in ref 20. However, IR measurements in a xenon solution by Durig and co-workers report an energy difference of 40 ± 3 cm^{-1} with the *gauche* conformer being more stable. This was determined by taking an average of nine conformer IR line pairs (three *gauche* bands and three *anti* bands) where the nine values comprise a minimum of 17 ± 5 cm^{-1} and a maximum of 63 ± 14 cm^{-1}.[21] This is the value employed in the CDMS database. More recently, Kerkeni and co-workers, using CCSD(T) − F12 ab initio methods, determined that the *gauche* and *anti* conformers have a relative energy difference of 22.6 cm^{-1} and a G-A interconversion barrier of 1215.3 cm-1 with the *gauche* conformer being the lower energy species.[22] However, these very small energy differences make their precise determination as well as the overall energy ordering challenging for both theory and experiment.

Indeed, these rigorous models and high-level calculations could be greatly improved with additional input from experimental measurements as to the isomer and conformer-specific energy ordering, rates of reactions, and product branching ratios associated with the chemistry occurring in and on icy grains. Although not inherently structure-specific, the study of ices using Fourier transform infrared spectroscopy (FTIR) and mass spectrometry (MS) has yielded profound insight into the chemistry of icy grains.[23−32] Additional techniques have recently emerged that offer isomer and conformer-specific probes of ice chemistry such as that reported by Theulé et al.,[33] Yocum et al.,[34,35] and recently by our group.[36] The former approaches employ radiation in the THz and mm-wave regimes, in a way analogous to detection by radiotelescopes, to study molecules that have desorbed from ices. In the ISM, molecules may sublime over a range of characteristic temperatures as they approach a protostar. Although inherently structure-specific and thus essential for the detection of new molecular species, rotational spectroscopy is less sensitive than other detection methods owing to the strong temperature dependence of the partition function, which is significant in the temperature regime over which most complex organic molecules (COMs) sublime. Here, COM is taken in the astrophysical context to mean molecules with six or more atoms. However, one may greatly improve the sensitivity of this detection approach by reducing the temperature of the molecules under investigation, as we show in our instrument, CPICE (chirped-pulse rotational spectroscopy of ices). This new approach incorporates a buffer gas cell to cool molecules desorbing from an ice to ∼25 K for sensitive detection by chirped-pulse spectroscopy in the mm-wave regime. While cold, these molecules are subjected to broadband excitation pulses resulting in the detection of highly resolved molecular signals via rotational transitions immediately following desorption.[37] In previous work, we showed the successful application of this technique for the gas-phase injection of *n*-PrCN, where we examined *anti*-*n*-PrCN and *gauche*-*n*-PrCN to determine the rotational temperature of molecules within a 25 K cell.[38] In our most recent work with *normal*- and *iso*-propanol (PrOH), we applied CPICE to study molecules desorbing from an ice surface over the course of temperature-programmed desorption (TPD).[36] This previous work revealed surprising conformer-specific desorption profiles and quantified the relative abundances of conformers and isomers following both room-temperature gas-phase injection and separately following TPD of PrOH ices generated at 4 K. The results showed that the relative conformer yield varied dramatically during desorption, likely reflecting the composition of the ice itself. In the present paper, we report the conformer distributions of *n*-PrCN following room-temperature gas-phase injection into a 25 K buffer gas cell and following sublimation of these same species from an ice. We also report our own measurement of the energy difference between the *anti* and *gauche* species determined from the abundance ratios observed in the room-temperature gas-phase injection experiments with detection by broadband rotational spectroscopy.

EXPERIMENTAL SECTION

The apparatus employed to carry out these experiments has been previously described in detail[38] and thus only a brief description is provided here. In CPICE, ices are generated, sublimed, buffer gas cooled, and detected within the same

https://doi.org/10.1021/acsearthspacechem.3c00332
ACS Earth Space Chem. 2024, 8, 14−20

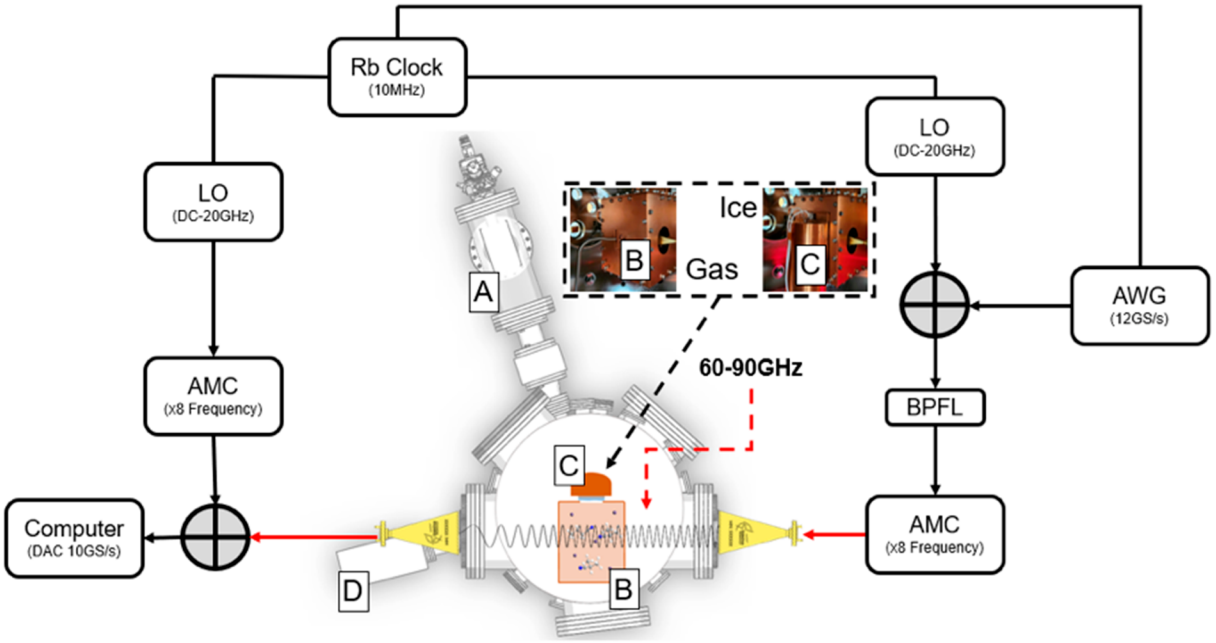

Figure 1. Diagram of the instrument and spectrometer components. (A) Electron gun, (B) buffer gas cell with room-temperature gas deposition stainless steel tube brought up to the orifice, and (C) rotatable, translatable copper rod containing the silver substrate brought up to the buffer gas cell. In the spectrometer, the upconversion side contains an arbitrary waveform generator (AWG) and local oscillator (LO), which generate the transition frequencies that are mixed before being sent through a band-pass filter (BPFL) and 8X frequency multiplier (AMC). The resulting radiation enters the chamber and BGC through a sapphire window. Following coherent excitation, the free induction decay is captured by a receiver horn directly mounted onto the BGC, which is ultimately interfaced with the atmosphere side via waveguides for downconversion. The FID frequency is mixed with a separate LO, downconverted with a second 8X AMC, and ultimately sent into a 10 GS/s digitzer.

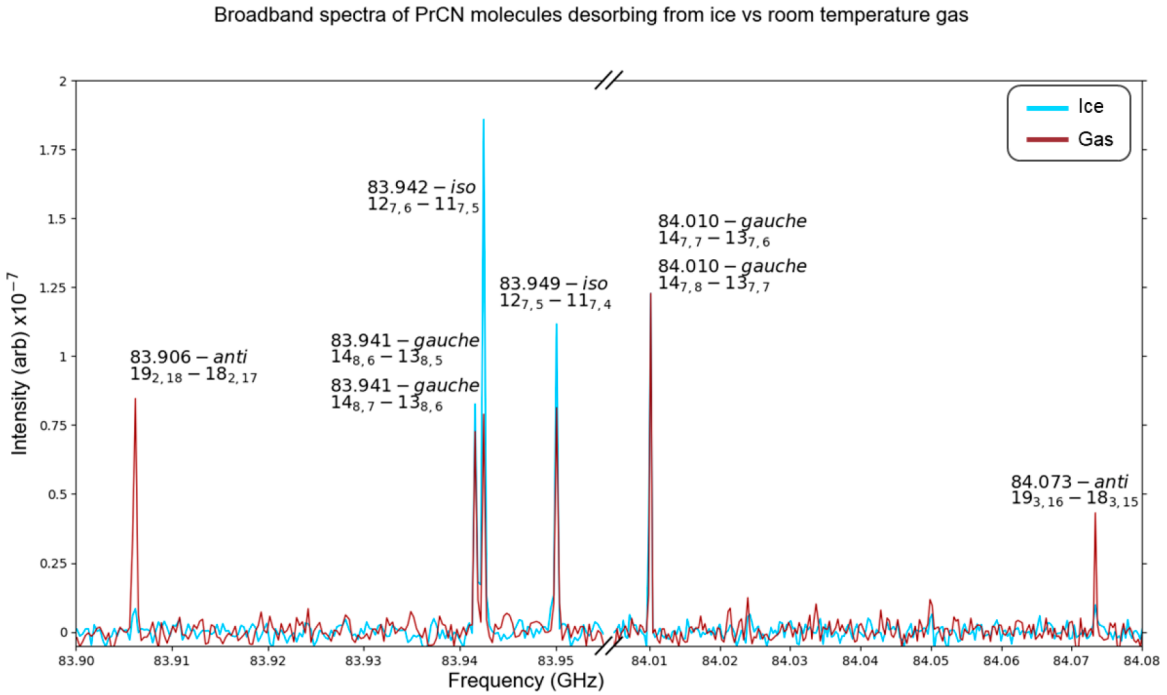

Figure 2. Comparison of the broadband rotational spectra of PrCN molecules from room-temperature gas injection (red) and from molecules desorbing from an ice during slow warmup (blue). The room-temperature gas spectra are scaled up to the 84.010 GHz *gauche-n*-PrCN signal in the spectra of molecules desorbing from an ice.

custom-built stainless steel UHV (1×10^{-10} Torr) apparatus as shown in Figure 1. In these experiments, we examine the conformer distribution of *a:g n*-PrCN following direct room-temperature gas-phase injection into the 25 K buffer gas cell (BGC) versus when those same species are introduced into the cell via sublimation from an ice. In the gas phase, varying flow rates of *n*-PrCN (0.03−0.08 sccm) are introduced into the BGC, which is cooled to 25 K by a closed-cycle He cryostat. Precooled Ne gas is introduced into the cell at a flow rate of 6 sccm for efficient cooling of the room-temperature molecules

https://doi.org/10.1021/acsearthspacechem.3c00332
ACS Earth Space Chem. 2024, 8, 14−20

introduced. A second coldhead is mounted to the bottom of the CPICE apparatus. Here, ices are generated at 4 K by slowly depositing *n*-PrCN onto a silver substrate attached to this coldhead. Following deposition, the ice stage is raised to the entry orifice of the 25 K BGC. TPD then begins at a ramping rate of 2 K/min using a 50 ohm cartridge heater placed behind the substrate. As the substrate reaches the desorption temperature of PrCN, the molecules sublime and enter the BGC for prompt cooling via collisions with cold Ne atoms, where they experience continuous excitation and detection with broadband radiation in the mm-wave regime. Figure 1 includes a schematic of the spectrometer employed in this work. A broadband scan sweeping up and down from 83.88 to 84.13 GHz was employed as this region was rich with transitions for all species of PrCN containing many lines well within the range of our limit of detection.

RESULTS AND DISCUSSION

Broadband spectra of *n*-PrCN injected both from a room-temperature gas-phase sample and following desorption from an ice surface are given in Figure 2. The gas-phase injection spectrum (red) was obtained by averaging for 1 h at near-continuous operating conditions. The spectrum shown following sublimation from the ice (blue) was obtained by averaging the spectra across the sublimation temperature region (160−220 K). The same spectrometer and data acquisition conditions as described above were used in both experiments. Both spectra are background subtracted and corrected for chirp power (when needed) and line strength factors (see the Supporting Information for additional details). A number of differences in the conformer distributions are observed between these two experiments. The gas-phase-injected spectrum in Figure 2 (red trace) contains several transitions associated with both the *anti* and *gauche* *n*-PrCN species, the relative abundances of which are further discussed below. However, following desorption from ice, the *anti* abundance is drastically reduced.

To gain a more detailed picture of the conformer-specific desorption behavior, Figure 3 shows the average TPD profiles of the *n*-PrCN conformers. During TPD, the rise and fall of the signals of molecules entering the buffer gas cell off the ice is observed within 160−220 K, consistent with the reported 160 K desorption temperature. In order to determine the fractional populations of each species, the *n*-PrCN conformers are treated as individual species rather than two variants of the same molecule, as discussed in the Supporting Information.

With this, the *a*:*g* ratio can be expressed in terms of the detected signals as

$$\frac{N_a}{N_g} = \frac{\left(\frac{I_a Q_a}{e^{-E_a/kT_{rot}} S\mu_a^2}\right)}{\left(\frac{I_g Q_g}{e^{-E_g/kT_{rot}} S\mu_g^2}\right)} \quad (1)$$

where N is the conformer population, I is the signal intensity, Q is the rotational partition function, E is the rotational energy (exclusive of conformer origin energy), T_{rot} is the rotational temperature, and $S\mu^2$ is the line strength factor. For all of these, the subscripts indicate the respective conformer.

Table 1 presents the relative abundances calculated as described above for the conformers in the gas phase following room-temperature gas injection and following desorption from ice, the former of which may be used to determine the conformer energy difference of the *n*-PrCN species. Or, if the relative energy is known, we can determine an effective "conformer temperature" as discussed below.

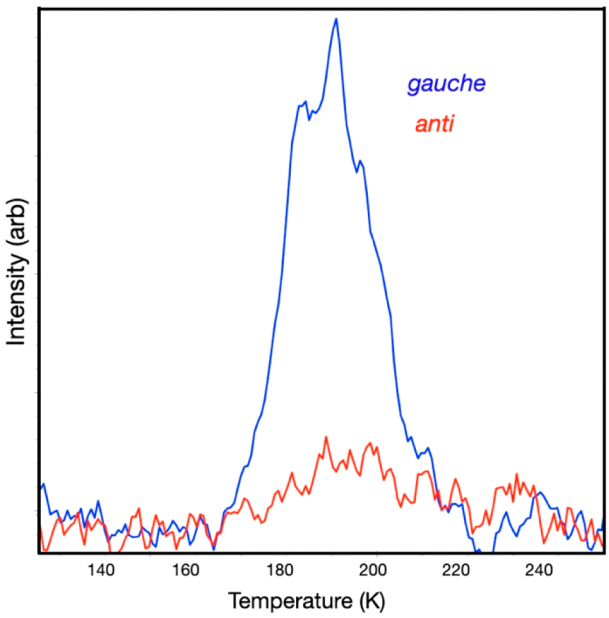

Figure 3. Temperature-programmed desorption profiles of the *n*-PrCN conformers averaged across multiple experiments, where each profile is an average of several transitions of a single conformer.

Table 1. Relative Abundances of *n*-PrCN Conformers Following RT Gas-Phase Injection and Sublimation from an Ice

	a/*g*
RT gas-phase injection	0.31 ± 0.09
TPD from ice	0.041 ± 0.001

First, we examine the room-temperature result to infer the relative conformer energy. This assumes there is no relaxation of the conformer distribution from the gas phase in the BGC, which is reasonable given the calculated ∼1250 cm^{-1} barrier to interconversion. The relative abundances between the two conformers (assuming they are rotationally thermalized) may be written as

$$\frac{N_a}{N_g/2} = \frac{e^{-E_a/kT_{conf}}}{e^{-E_g/kT_{conf}}} \quad (2)$$

where N_a and N_g are the *anti* and *gauche* conformer populations, respectively, E_a and E_g are the relative energies of the *anti* and *gauche* conformers, respectively, and the factor of 2 accounts for the statistical weight of the *gauche* species (there are two equivalent but distinct forms). T_{conf} is a characteristic conformer temperature, and we assume T_{conf} = 300 K for the room-temperature injection. The conformer temperature is defined here as the temperature describing the relative abundance of the species in consideration, analogous to a vibrational temperature. Since the conformer energies are relative, we set E_g = 0, and the sign of the *anti* energy will determine which is the lower energy species. It is clear, though, as the *anti* species has a lower abundance, it must be the higher energy conformer. This reduces eq 2 to

https://doi.org/10.1021/acsearthspacechem.3c00332
ACS Earth Space Chem. 2024, 8, 14−20

$$\frac{N_a}{N_g/2} = e^{-E_a/kT_{conf}} \quad (3)$$

With this, based on the room-temperature measurement, we find the relative energy difference between the *anti* and *gauche* conformers to be 97 ± 21 cm^{-1} with the *anti* being the higher energy species.

We compare our results with those of previous experiments that explored the relative energies using various spectroscopic and theoretical methods. Durig et al.[21] examined the IR spectra for several bands of PrCN dissolved in xenon at varying temperatures from 213.5 to 173 K supported by calculations at the MP2/6-311+G(2df,2pd) level of theory. From this, they obtained an experimental relative energy of 40 ± 3 cm^{-1} for the *anti* species, while the ab initio and hybrid DFT methods calculations ranged from −37 to 186 cm^{-1}. They note that overtones and combination bands lead to convoluted spectra and high uncertainties associated with the final numbers. Ultimately, they report a lower limit on the energy difference of 40 cm^{-1}, with *gauche* being the more stable conformer. This is currently given in CDMS. This same group performed related experiments in a krypton solution and found similar relative energies but with much greater uncertainties. They also reported a Raman study of the pure liquid from −105 to 25 °C. From this, they obtained the *anti* energy as 93 ± 10 cm^{-1}, remarkably close to our value.

Tratteberg[39] and co-workers examined the *gauche:anti* ratios of room-temperature gas-phase PrCN using gaseous electron diffraction. The conformer distribution derived from the radial distribution curves obtained was determined to be 75.1% *gauche* and 24.9% (± 6%) *anti,* corresponding to an energy difference of 84.6 cm^{-1}, again quite close to our value and to Durig's number for the pure liquid. The enhanced stability of the *gauche* is suggested to arise from the attractive interaction between its methyl group and the π-electron of the triple bond. One point worthy of note is that the Durig result employed by CDMS was obtained in xenon solution, while their neat liquid number and direct gas-phase values from us and Tratteberg are all in good agreement, suggesting a significantly higher energy for the *anti* conformer. This difference will have an impact on the isomer (*normal* to *iso*) PrCN abundances inferred from astronomical observations.

Given the relative energy of the *anti* and *gauche* species, we can relate the relative abundances of the species observed to a specific conformer temperature, although this may have little to do directly with the temperature of the ice, given the high barrier to interconversion. We first assume an energy difference of 97 cm^{-1} as obtained above. Based on the integrated TPD, the conformer temperature for the molecules desorbing from the ice is thus determined to be 55.8 ± 11.8 K, much lower than the desorption temperature of 175−223 K. Alternatively, we can use the 40 cm^{-1} *anti* energy employed in CDMS to obtain a conformer temperature of 18 K.

In addition to experiments aimed at determining the conformer energies, the ice composition of *n*-PrCN has also been extensively explored. Depending upon the temperature and condition from which it is generated, whether a liquid or a gas, and the rate at which the ice is warmed for gas-phase detection, the observed conformer distributions vary. Durig et al. reported that when condensing *n*-PrCN from the gas phase on to a cold substrate held at ∼77K, it preferentially forms an ice which contains entirely the *gauche* conformer after thorough annealing. However, when the *n*-PrCN solid was made from liquid PrCN instead of gas, it contained entirely the *anti* conformer.

Ishii and co-workers also examined the conformer distribution of *n*-PrCN in liquid, glass, and crystalline phases using both Raman spectroscopy and X-ray diffraction.[40] They reported that when PrCN vapor is condensed onto a cold substrate, it initially forms an amorphous solid. This amorphous solid shares a conformer distribution with the liquid phase, with the *anti* conformer still being present in an amount comparable to the *gauche.* They showed qualitatively how the conformer distribution in the amorphous solid evolves with temperature as it was heated from 20 K as a vapor deposited solid and cooled beyond the melting point from room temperature as a liquid, although they did not report the rate of warming. They highlighted two critical temperatures for the solids: the glass transition temperature, reported at the time as 97 K,[41] and the crystallization temperature. They first obtained an *n*-PrCN crystalline solid by the process of annealing. Then by comparison with its Raman spectra, they reported that the liquid, when cooled down, crystallizes at ∼130 K, while the solid made from the vapor on a cold substrate, when heated up, crystallizes at ∼120 K. In both scenarios, they find the two solids share a similar conformer distribution (with the *anti* conformer still comparably present) up until the crystallization temperature. Once within the bounds of crystallization, they observed that the *anti* bands diminish in the spectra while the *gauche* bands grow in intensity, with the result being a predominantly *gauche*-PrCN crystalline solid. In that work they highlighted the ability of the amorphous PrCN to resist crystallization after exceeding the glass transition temperature, which was considered novel given that previous experiments showed that amorphous solids made from vapor condensed onto a cold substrate undergo crystallization without manifesting a glass transition.[42] This glass persistence was ascribed to the high barrier to conformer relaxation.

In our experiments examining the TPD of *n*-PrCN via CPICE, we observe the *anti* species in low but measurable abundance at a temperature above the crystallization temperature (∼170 K). Guided by the previous findings described above, we attribute this to the sample not undergoing conformational relaxation completely during the warm up. Moreover, unlike the TPD we observed from propanol ice,[36] here we do not see changing relative conformer abundances, suggesting the ice is here dominated by a single form.

CONCLUSION

The conformer distributions of buffer gas cooled *n*-PrCN were studied by broadband rotational spectroscopy following room-temperature gas-phase injection and over the course of temperature-programmed desorption from an ice. On the basis of the conformer ratios observed in the latter experimental configuration, our measurements yield an energy difference of ∼97 ± 21 cm^{-1} with the *gauche* conformer being the lower energy species. Given this energy difference, we determine a conformer temperature of 55.8 ± 11.8 K for those species that desorb from an ice, which is much lower than the desorption temperature of 170 K. This shows that the *anti* is in much lower abundance than would be expected from the room-temperature deposition and the 170 K desorption based on those temperatures alone. The low conformer temperature may arise owing to relaxation to the *gauche* species as the ice is warmed, as seen in the Raman studies discussed above,

https://doi.org/10.1021/acsearthspacechem.3c00332
ACS Earth Space Chem. 2024, 8, 14−20

followed by desorption that preserves the conformer identity. An alternative explanation, however, is that there is some conformer relaxation from the *anti* species that participates in the desorption process. This is an interesting subject for further investigation.

To our knowledge, current astrochemical models and interpretation of astronomical observations assume an energy difference of ∼40 cm^{-1}. Given our findings, in addition to previous reports as summarized above, this is likely an underestimation and should be reconsidered in branching ratio determinations in both the wide range of astrochemical models and for interpreting observations.

■ ASSOCIATED CONTENT

Supporting Information

The Supporting Information is available free of charge at https://pubs.acs.org/doi/10.1021/acsearthspacechem.3c00332.

Determination of conformer ratios, calculation of the conformer-specific partition functions, and Table S1 summarizing the rotational transitions probed (PDF)

■ AUTHOR INFORMATION

Corresponding Author

Bernadette M. Broderick − *Department of Chemistry, University of Missouri, Columbia, Missouri 65211, United States*; orcid.org/0000-0003-0232-4239; Email: broderickbm@missouri.edu

Authors

Anudha Kanaherarachchi − *Department of Chemistry, University of Missouri, Columbia, Missouri 65211, United States*

Travis Hager − *Department of Chemistry, University of Missouri, Columbia, Missouri 65211, United States*

Quentin Borengasser − *Department of Chemistry, University of Missouri, Columbia, Missouri 65211, United States*

Complete contact information is available at: https://pubs.acs.org/10.1021/acsearthspacechem.3c00332

Notes

The authors declare no competing financial interest.

■ ACKNOWLEDGMENTS

We gratefully acknowledge the University of Missouri for generous startup funds and the National Science Foundation Advanced Manufacturing Program, Grant 2314347. We thank G. E. Hall for the design and implementation of the CPICE data acquisition software and A. G. Suits for many helpful discussions.

■ REFERENCES

(1) Müller, H. S. P.; Thorwirth, S.; Roth, D. A.; Winnewisser, G. The Cologne Database for Molecular Spectroscopy, CDMS. *A&A* **2001**, *370* (3), L49−L52.

(2) Müller, H. S. P.; Schlöder, F.; Stutzki, J.; Winnewisser, G. The Cologne Database for Molecular Spectroscopy, CDMS: a useful tool for astronomers and spectroscopists. *J. Mol. Struct.* **2005**, *742* (1), 215−227.

(3) Glavin, D. P.; McLain, H. L.; Dworkin, J. P.; Parker, E. T.; Elsila, J. E.; Aponte, J. C.; Simkus, D. N.; Pozarycki, C. I.; Graham, H. V.; Nittler, L. R.; Alexander, C. M. O. D. Abundant extraterrestrial amino acids in the primitive CM carbonaceous chondrite Asuka 12236. *Meteoritics & Planetary Science* **2020**, *55* (9), 1979−2006.

(4) Ehrenfreund, P.; Glavin, D. P.; Botta, O.; Cooper, G.; Bada, J. L. Extraterrestrial amino acids in Orgueil and Ivuna: Tracing the parent body of CI type carbonaceous chondrites. *Proc. Natl. Acad. Sci. U. S. A.* **2001**, *98* (5), 2138−2141.

(5) Elsila, J. E.; Dworkin, J. P.; Bernstein, M. P.; Martin, M. P.; Sandford, S. A. Mechanisms of Amino Acid Formation in Interstellar Ice Analogs. *Astrophysical Journal* **2007**, *660* (1), 911−918.

(6) Botta, O.; Bada, J. L. EXTRATERRESTRIAL ORGANIC COMPOUNDS IN METEORITES. *Surveys in Geophysics* **2002**, *23* (5), 411−467.

(7) Belloche, A.; Garrod, R. T.; Müller, H. S. P.; Menten, K. M.; Comito, C.; Schilke, P. Increased complexity in interstellar chemistry: detection and chemical modeling of ethyl formate and *n*-propyl cyanide in Sagittarius B2(N). *Astronomy & Astrophysics* **2009**, *499* (1), 215−232.

(8) Belloche, A.; Garrod, R. T.; Müller, H. S. P.; Menten, K. M. Detection of a branched alkyl molecule in the interstellar medium: iso-propyl cyanide. *Science* **2014**, *345* (6204), 1584−1587.

(9) Pagani, L.; Favre, C.; Goldsmith, P. F.; Bergin, E. A.; Snell, R.; Melnick, G. The complexity of Orion: an ALMA view. *Astronomy & Astrophysics* **2017**, *604*, A32.

(10) Hasegawa, T. I.; Herbst, E. Three-phase chemical models of dense interstellar clouds: gas, dust particle mantles and dust particle surfaces. *Mon. Not. R. Astron. Soc.* **1993**, *263* (3), 589−606.

(11) Garrod, R. T.; Herbst, E. Formation of methyl formate and other organic species in the warm-up phase of hot molecular cores. *Astron. Astrophys.* **2006**, *457*, 927−936.

(12) Garrod, R. T.; Weaver, S. L. W.; Herbst, E. Complex Chemistry in Star-forming Regions: An Expanded Gas-Grain Warm-up Chemical Model. *Astrophysical Journal* **2008**, *682*, 283−302.

(13) Garrod, R. T.; Pauly, T. On the formation of CO2 and other interstellar ices. *Astrophysical Journal* **2011**, *735* (1), 15.

(14) Garrod, R. T. A Three-phase Chemical Model of Hot Cores: The Formation of Glycine. *Astrophysical Journal* **2013**, *765*, 60.

(15) Garrod, R. T.; Belloche, A.; Müller, H. S. P.; Menten, K. M. Exploring molecular complexity with ALMA (EMoCA): Simulations of branched carbon-chain chemistry in Sgr B2(N). *Astronomy & Astrophysics* **2017**, *601*, A48.

(16) Belloche, A.; Garrod, R. T.; Zingsheim, O.; Müller, H. S. P.; Menten, K. M. Interstellar detection and chemical modeling of iso-propanol and its normal isomer. *Astronomy & Astrophysics* **2022**, *662*, A110.

(17) Kerkeni, B.; Gámez, V.; Ouerfelli, G.; Senent, M. L.; Feautrier, N. Propyl-cyanide isomer formation on interstellar ices from radical association: a quantum theoretical study. *Mon. Not. R. Astron. Soc.* **2023**, *522* (4), 5254−5266.

(18) Hirota, E. Rotational isomerism and microwave spectroscopy. II. The microwave spectrum of butyronitrile. *J. Chem. Phys.* **1962**, *37* (12), 2918−2920.

(19) Wlodarczak, G.; Martinache, L.; Demaison, J.; Marstokk, K.-M.; Møllendal, H. Rotational spectrum of butyronitrile: Dipole moment, centrifugal distortion constants and energy difference between conformers. *J. Mol. Spectrosc.* **1988**, *127* (1), n/a.

(20) Ellingsen, B. H.; Marstokk, K. M.; Møllendal, H. Microwave spectrum, conformational equilibrium, intramolecular hydrogen bonding, thermodynamic parameters, dipole moments and centrifugal distortion of 2-amino-1-propanol (alaninol). *J. Mol. Struct.* **1978**, *48* (1), 9−23.

(21) Durig, J. R.; Drew, B. R.; Koomer, A.; Bell, S. Infrared and Raman spectra, conformational stability, ab initio calculations of structure and vibrational assignment of butyronitrile. *Phys. Chem. Chem. Phys.* **2001**, *3* (5), 766−775.

(22) Kerkeni, B.; Gámez, V.; Senent, M. L.; Feautrier, N. Understanding propyl cyanide and its isomers formation: ab initio study of the spectroscopy and reaction mechanisms. *Phys. Chem. Chem. Phys.* **2019**, *21* (42), 23375−23384.

(23) Maity, S.; Kaiser, R. I.; Jones, B. M. Infrared and reflectron time-of-flight mass spectroscopic study on the synthesis of glycolaldehyde in methanol (CH 3 OH) and methanol−carbon monoxide (CH 3 OH−CO) ices exposed to ionization radiation. *Faraday Discuss.* **2014**, *168*, 485−516.
(24) Góbi, S.; Crandall, P. B.; Maksyutenko, P.; Förstel, M.; Kaiser, R. I. Accessing the Nitromethane (CH3NO2) Potential Energy Surface in Methanol (CH3OH)−Nitrogen Monoxide (NO) Ices Exposed to Ionizing Radiation: An FTIR and PI-ReTOF-MS Investigation. *J. Phys. Chem. A* **2018**, *122* (9), 2329−2343.
(25) Shulenberger, K. E.; Zhu, J. L.; Tran, K.; Abdullahi, S.; Belvin, C.; Lukens, J.; Peeler, Z.; Mullikin, E.; Cumberbatch, H. M.; Huang, J.; et al. Electron-Induced Radiolysis of Astrochemically Relevant Ammonia Ices. *ACS Earth and Space Chemistry* **2019**, *3* (5), 800−810.
(26) Schmidt, F.; Swiderek, P.; Bredehöft, J. H. Electron-Induced Processing of Methanol Ice. *ACS Earth and Space Chemistry* **2021**, *5* (2), 391−408.
(27) Oba, Y.; Tomaru, T.; Lamberts, T.; Kouchi, A.; Watanabe, N. An infrared measurement of chemical desorption from interstellar ice analogues. *Nature Astronomy* **2018**, *2* (3), 228−232.
(28) Muñoz Caro, G. M.; Schutte, W. A. UV-photoprocessing of interstellar ice analogs: New infrared spectroscopic results. *Astronomy & Astrophysics* **2003**, *412* (1), 121−132.
(29) Esmaili, S.; Bass, A. D.; Cloutier, P.; Sanche, L.; Huels, M. A. Glycine formation in CO2:CH4:NH3 ices induced by 0−70 eV electrons. *J. Chem. Phys.* **2018**, *148* (16), n/a DOI: 10.1063/1.5021596.
(30) Oberg, K. I.; van Dishoeck, E. F.; Linnartz, H.; Andersson, S. The Effect of H_2O on Ice Photochemistry. *Astrophysical Journal* **2010**, *718*, 832.
(31) Gudipati, M. S.; Yang, R. In-situ probing of radiation-induced processing of organics in astrophysical ice analogs—Novel laser desorption laser ionization time-of-flight mass spectroscopic studies. *Astrophysical Journal Letters* **2012**, *756* (1), L24.
(32) Ioppolo, S.; Fedoseev, G.; Chuang, K. J.; Cuppen, H. M.; Clements, A. R.; Jin, M.; Garrod, R. T.; Qasim, D.; Kofman, V.; Van Dishoeck, E. F.; Linnartz, H. A non-energetic mechanism for glycine formation in the interstellar medium. *Nature Astronomy* **2021**, *5* (2), 197−205.
(33) Theulé, P.; Endres, C.; Hermanns, M.; Bossa, J.-B.; Potapov, A. High-Resolution Gas Phase Spectroscopy of Molecules Desorbed from an Ice Surface: A Proof-of-Principle Study. *ACS Earth and Space Chemistry* **2020**, *4* (1), 86−91.
(34) Yocum, K. M.; Smith, H. H.; Todd, E. W.; Mora, L.; Gerakines, P. A.; Milam, S. N.; Widicus Weaver, S. L. Millimeter/Submillimeter Spectroscopic Detection of Desorbed Ices: A New Technique in Laboratory Astrochemistry. *J. Phys. Chem. A* **2019**, *123* (40), 8702−8708.
(35) Wilkins, O.; Yocum, K.; Milam, S.; Gerakines, P.; Thompson, W.; Cruz-Diaz, G.; Widicus Weaver, S. Rotational Spectroscopy as a Sublime Tool for Identifying Organic Products of UV-Photolyzed Cosmic Ice Analogues. *Presentation #134.03 in the session Laboratory Astrophysics (LAD) Division Meeting: The Salty Solar System II* **2022**, *54* (6), n/a.
(36) Borengasser, Q.; Hager, T.; Kanaherarachchi, A.; Troya, D.; Broderick, B. M. Conformer-Specific Desorption in Propanol Ices Probed by Chirped-Pulse Millimeter-Wave Rotational Spectroscopy. *J. Phys. Chem. Lett.* **2023**, *14* (29), 6550−6555.
(37) Gurusinghe, R. M.; Dias, N.; Broderick, B. M. Buffer gas cooling for sensitive rotational spectroscopy of ice chemistry: A proposal. *Chem. Phys. Lett.* **2021**, *762*, 138125.
(38) Radhakrishnan, S.; Hager, T.; Kanaherarachchi, A.; Williams, C.; Hall, G. E.; Broderick, B. M. Buffer gas cooled ice chemistry. I. Buffer gas cell and mm-wave spectrometer. *J. Chem. Phys.* **2022**, *157* (15), n/a DOI: 10.1063/5.0111792.
(39) Traetteberg, M.; Bakken, P.; Hopf, H. Structure and conformation of gaseous butyronitrile: C−H···π interaction? *J. Mol. Struct.* **2000**, *556* (1), 189−196.
(40) Ishii, K.; Nakayama, H.; Koyama, K.; Yokoyama, Y.; Ohashi, Y. Molecular Conformation of Butanenitrile in Gas, Liquid, Glass, and Crystalline States: In Relation to the Stability of the Glass State. *Bull. Chem. Soc. Jpn.* **1997**, *70* (9), 2085−2091.
(41) Hikawa, H.; Oguni, M.; Suga, H. Construction of an adiabatic calorimeter for a vapor-deposited sample and thermal characterization of amorphous butyronitrile. *J. Non-Cryst. Solids* **1988**, *101* (1), 90−100.
(42) Ishii, K.; Nakayama, H.; Yoshida, T.; Usui, H.; Koyama, K. Amorphous State of Vacuum-Deposited Benzene and Its Crystallization. *Bull. Chem. Soc. Jpn.* **1996**, *69* (10), 2831−2838.

https://doi.org/10.1021/acsearthspacechem.3c00332
ACS Earth Space Chem. 2024, 8, 14−20